Available online at www.sciencedirect.com
SCIENCE DIRECT
Optics Communications 264 (2006) 63–69
OPTICS COMMUNICATIONS
www.elsevier.com/locate/optcom

Binary polarization pupil filter: Theoretical analysis and experimental realization with a liquid crystal display

Ignacio Moreno [a,*], Claudio Iemmi [b], Juan Campos [c], María J. Yzuel [c]

[a] Departamento de Ciencia y Tecnología de Materiales, Universidad Miguel Hernández, Elche E03202, Spain
[b] Departamento de Física, F.C.E. y N, Universidad de Buenos Aires, Argentina
[c] Departamento de Física, Universidad Autónoma de Barcelona, Bellaterra, Spain

Received 14 December 2005; accepted 7 February 2006

Abstract

The Jones matrix formalism has been applied to evaluate the response of an optical system when a non-uniform polarizing pupil is introduced. With this formalism we analyze and experimentally demonstrate the properties of a binary polarization pupil filter having two regions with two orthogonal linear polarization orientations. We first study the case when no analyzer is placed behind the pupil filter, and both, the transversal and the axial behavior are described in terms of the intensity and the local state of polarization. Then it is shown how the response of the optical system can be easily changed through the orientation of an analyzer placed behind the pupil. We experimentally verified the theory using a twisted nematic liquid crystal display, which produces two orthogonal linear polarization states for two different addressed voltages.

PACS: 42.25.−p; 42.25.Ja; 42.30.Kq; 42.30.Va; 42.79.Kr; 42.30.Lr

Keywords: Polarization; Apodization; Liquid crystal displays

1. Introduction

Non-uniform pupil filters placed on the exit pupil of an optical system produce effects on the point spread function (PSF), both in the transverse plane, generating apodization or superresolution [1], and axially, varying the depth of focus [2]. Usually amplitude-only or phase-only pupil filters are considered. These pupil filters can be made programmable by using a liquid crystal spatial light modulator (LC-SLM) [3–5]. In these cases the LC-SLM must be configured in order to produce an amplitude-only or phase-only modulation versus the applied voltage. These situations can be obtained through the polarization configuration of the display [6–8]. However, liquid crystal devices can be also employed to control the state of polarization of the emerging light [9], and pixelated LC-SLMs have been used to generate spatial polarization patterns [10].

On the other side, the use of polarization elements in the design of pupil filters has been theoretically proposed. For instance, in Refs. [11,12] polarizer masks were designed to be coated onto a lens, and the intensity of the PSF in the image plane was studied in terms of their orientation. In Ref. [13] the influence of the birefringence caused by rotationally symmetric stress distribution in a high-resolution projection optical system was investigated. More recently, the use of a uniaxial crystal to produce a phase-only pupil filter has been proposed [14]. Finally, in Ref. [15] it is proposed the use of half-wave plates cut in four quadrants to produce pseudoradial polarized beams.

The aim of this work is to use the polarization control properties of a liquid crystal display for the realization of a polarization pupil mask. The paper is organized as follows: in Section 2 we use the combination of the standard Jones matrix formalism with the Fourier transform to

* Corresponding author. Tel.: +34966658409; fax: +34966658602.
E-mail address: i.moreno@umh.es (I. Moreno).

0030-4018/$ - see front matter © 2006 Elsevier B.V. All rights reserved.
doi:10.1016/j.optcom.2006.02.016

analyze the diffraction produced by a spatially variant polarization pupil filter. In particular, we consider a rotationally symmetric binary polarization mask, consisting in an inner disk that transmits a linear polarization, surrounded by an annulus of equal area, which transmits the orthogonal linear polarization. In Section 3, we study the response of this pupil filter in two situations. Firstly, we consider the case when no analyzer is placed behind the filter. We calculate the distribution of the intensity and the state of polarization in the focal plane of the optical system, and also in some defocused planes. Secondly, we consider a linear polarizer placed behind the pupil mask, and we show how the properties of the pupil filter can be easily changed by a rotation of this analyzer element. Finally, in Section 4 we experimentally demonstrate all these results with the aid of a twisted nematic LC-SLM. We use a configuration of the display that, for the same input polarization, produces two orthogonal linear polarizations for two different addressed gray levels. Therefore, we experimentally reproduce the spatial polarization distribution of the pupil mask and measure its focusing properties. In Section 5, we present the conclusions of the work.

2. Rotationally symmetric polarization pupil filters

A spatially variant polarization diffractive element can be described by means of a Jones matrix $\mathbf{f}(x, y)$ where each element of the matrix $f_{ij}(x, y)$, being $i, j = 1, 2$, depends on the spatial coordinates (x, y). The diffracted field can be calculated as the Jones vector $V_1(u, v) = \mathbf{F}(u, v)V_0$, where V_0 is the Jones vector describing the polarization state of the incident beam, (u, v) are the spatial frequencies and $\mathbf{F}(u, v)$ is a Jones matrix whose elements F_{ij} are calculated as $F_{ij}(u, v) = \mathrm{FT}[f_{ij}(x, y)]$, being FT the Fourier transform operation [16].

We consider an optical system with a polarization mask with rotational symmetry. The pupil can be described with a Jones matrix $\mathbf{f}(x, y) = \mathbf{f}(r)$ whose elements $f_{ij}(r)$ only depend on the radial coordinate r. Then, the response of the optical system in the image space is described by a Jones matrix $\mathbf{F}(\rho, W_{20})$ whose elements F_{ij} are given by the Fourier–Bessel transform of each element $f_{ij}(r)$ of the matrix $\mathbf{f}(r)$, i.e.:

$$F_{ij}(\rho, W_{20}) = \int_0^1 f_{ij}(r) \exp[\mathrm{i}2\pi W_{20} r^2] J_0(2\pi r\rho) r \,\mathrm{d}r, \tag{1}$$

where r and ρ are the normalized radial coordinates in the pupil and in the image plane, respectively. The aperture is considered to have unit radius, and J_0 is the Bessel function of first class and zero order. We also introduce the defocus parameter W_{20} in order to compute the point spread function (PSF) at defocused planes. The laboratory radial (s) and axial (z) coordinates are related to ρ and W_{20} as

$$s = \frac{\lambda\rho}{\mathrm{NA}}, \quad z = \frac{2\lambda W_{20}}{\mathrm{NA}^2}, \tag{2}$$

where λ is the wavelength and NA is the numerical aperture [5].

The axial behavior can also be evaluated using the coordinate transformation $r^2 = t + 0.5$. Then, the functions F_{ij} along the axis $(\rho = 0)$ are obtained as

$$F_{ij}(\rho = 0, W_{20}) = \frac{\exp(\mathrm{i}\pi W_{20})}{2} \int_{-0.5}^{+0.5} f_{ij}(t) \exp[\mathrm{i}2\pi W_{20} t] \,\mathrm{d}t, \tag{3}$$

which shows the Fourier transform relation between $F_{ij}(0, W_{20})$ and $f_{ij}(t)$.

Let us note that the Jones matrix $\mathbf{F}(\rho, W_{20})$ simultaneously accounts for polarization and diffraction effects for a general nonuniform polarization pupil mask. The Jones vector describing the field in the image plane can be calculated as the product $V(\rho, W_{20}) = \mathbf{F}(\rho, W_{20})V_0$, where V_0 is the Jones vector describing the polarization of the beam incident on the optical system.

As an example we consider the case described in Fig. 1(a). The polarization pupil mask is composed of a circular aperture with a linear polarizer oriented horizontal, surrounded by an anular aperture with a linear polarizer oriented vertical. We consider the outer circle to have a radial coordinate $r_2 = 1$. In order to have the same area in both zones, the inner circle is selected to have a radius $r_1 = 1/\sqrt{2}$. The spatially variant Jones matrix describing this aperture is given by

$$\mathbf{f}(r) = \begin{pmatrix} \mathrm{circ}(r\sqrt{2}) & 0 \\ 0 & \mathrm{circ}(r) - \mathrm{circ}(r\sqrt{2}) \end{pmatrix}. \tag{4}$$

where $\mathrm{circ}(r) = 1$ if $r \leqslant 1$ and $\mathrm{circ}(r) = 0$ if $r > 1$ [17]. If we rewrite this Jones matrix in terms of the coordinate $t = r^2 - 0.5$, it is given by

$$\mathbf{f}(t) = \begin{pmatrix} \mathrm{rect}\left(\frac{t+0.25}{0.5}\right) & 0 \\ 0 & \mathrm{rect}\left(\frac{t-0.25}{0.5}\right) \end{pmatrix}. \tag{5}$$

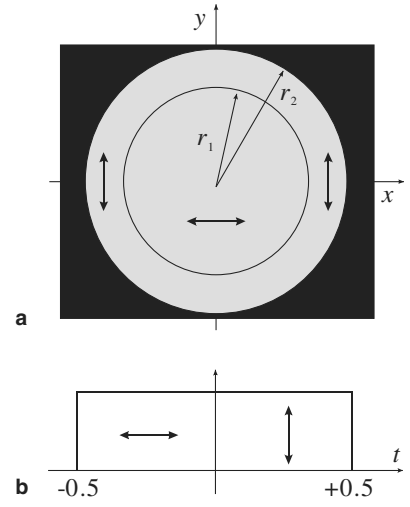

Fig. 1. (a) Binary polarization pupil filter (the arrows indicate the orientation of the polarizer transmission axis). (b) Radial polarizer distribution, in terms of the coordinate $t = r^2 - 0.5$.

This situation is described in Fig. 1(b). A polarizer oriented horizontal corresponds to values $t \in [-0.5, 0]$, while it is oriented vertical for values $t \in [0, +0.5]$.

The Jones matrix $\mathbf{F}(\rho)$ describing the best image plane ($W_{20} = 0$) is obtained [16] by Fourier transforming each term in Eq. (4), i.e.

$$\mathbf{F}(\rho) = \frac{1}{\rho}\begin{pmatrix} 2J_1(2\pi\rho/\sqrt{2}) & 0 \\ 0 & J_1(2\pi\rho) - 2J_1(2\pi\rho/\sqrt{2}) \end{pmatrix}. \tag{6}$$

where J_1 is the Bessel function of first class and first order. On the other hand, the Jones matrix $\mathbf{F}(W_{20})$ associated with the axial behavior is obtained by Fourier transforming the matrix elements in Eq. (5), i.e.,

$$\mathbf{F}(W_{20}) = \frac{1}{2}\mathrm{sinc}(W_{20}/2)\cdot\exp(+\mathrm{i}\pi W_{20}) \cdot \begin{pmatrix} \exp(-\mathrm{i}\pi W_{20}/2) & 0 \\ 0 & \exp(+\mathrm{i}\pi W_{20}/2) \end{pmatrix}. \tag{7}$$

These two Jones matrices simultaneously account for the polarization and diffraction properties in the image plane (Eq. (6)) and along the optical axis (Eq. (7)).

3. Focusing properties of the binary polarization pupil filter

In this section, we apply the above theory to evaluate the properties of the polarization pupil filter. We consider two situations: (1) No analyzer is placed behind the pupil filter. We evaluate the intensity distribution in the focusing region, but also the state of polarization, which is spatially variable. (2) An analyzer with orientation θ is placed behind the pupil mask. Then the filter response can be easily changed depending on the value of θ.

We consider illumination with linear polarized light oriented at 45° in order to have the same transmitted intensity in both areas of the polarization pupil filter. Therefore, the input normalized Jones vector is

$$V_0 = \frac{1}{\sqrt{2}}\begin{pmatrix} 1 \\ 1 \end{pmatrix}. \tag{8}$$

The Jones vector describing the light at the image plane is obtained by applying the usual Jones matrix multiplication using the Jones matrix in Eq. (6). The result is

$$V_1(\rho) = \mathbf{F}(\rho)\cdot V_0 = \frac{1}{\rho\sqrt{2}}\begin{pmatrix} 2J_1(2\pi\rho/\sqrt{2}) \\ J_1(2\pi\rho) - 2J_1(2\pi\rho/\sqrt{2}) \end{pmatrix}. \tag{9}$$

Fig. 2 shows the intensity distribution as a function of the radial coordinate ρ, calculated as $I(\rho) = V_1^{\dagger}(\rho)\cdot V_1(\rho)$. The curve named "NoA" corresponds to the case when no analyzer is placed behind the pupil. On top it is drawn the local state of polarization, which is always linearly polarized since there is no phase-shift between both components of the Jones vector $V_1(\rho)$ in Eq. (9). However, it rotates depending on the value of ρ. As a consequence the placement of an analyzer results in very different behavior depending on its orientation θ of its transmission axis.

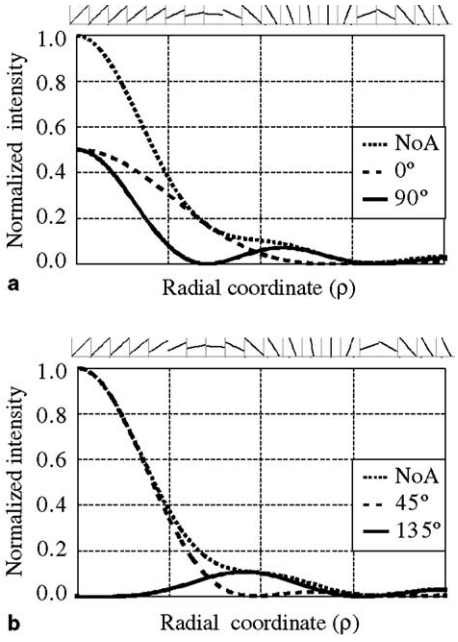

Fig. 2. Normalized intensity and local state of polarization (on top) in the best image plane ($W_{20} = 0$) as a function of the normalized radial coordinate ρ. The illumination is assumed linearly polarized at 45°. "NoA" corresponds to the case without analyzer. (a) $\theta = 0°$ and $\theta = 90°$. (b) $\theta = 45°$ and $\theta = 135°$.

In this situation, it is required to project the Jones vector in Eq. (9) into a linear polarizer with angle θ. The new Jones vector $V_1^A(\rho)$ is calculated as

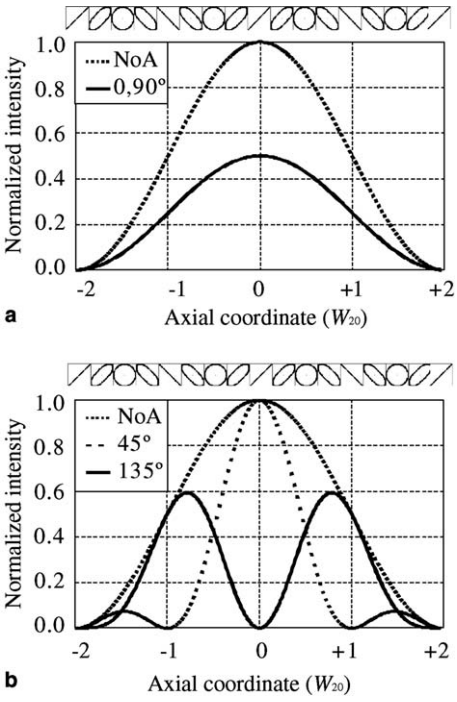

Fig. 3. Normalized intensity and local state of polarization (on top) as a function of the normalized axial coordinate W_{20}. The illumination is assumed linearly polarized at 45°. "NoA" corresponds to the case without analyzer. (a) $\theta = 0°$ and $\theta = 90°$. (b) $\theta = 45°$ and $\theta = 135°$.

$$V_1^A(\rho) = \mathbf{R}(-\theta)\mathbf{P_0}\mathbf{R}(+\theta)V_1(\rho), \tag{10}$$

where $\mathbf{P_0}$ is the Jones matrix for the linear polarizer oriented horizontal (along x axis), i.e.,

$$\mathbf{P_0} = \begin{pmatrix} 1 & 0 \\ 0 & 0 \end{pmatrix}, \tag{11}$$

and $\mathbf{R}(\theta)$ is the 2×2 rotation matrix, i.e.

$$\mathbf{R}(\theta) = \begin{pmatrix} \cos(\theta) & \sin(\theta) \\ -\sin(\theta) & \cos(\theta) \end{pmatrix}. \tag{12}$$

Fig. 2(a) shows the intensity distributions corresponding to the analyzer oriented at $\theta = 0°$ and $\theta = 90°$. In the first case only the central disk with aperture $1/\sqrt{2}$ transmits light and the result is the classical Airy pattern. When $\theta = 90°$ only the annulus transmits light and a hyperresolving effect is produced. Fig. 2(b) shows the case when $\theta = 45°$ and $\theta = 135°$. In the first case both areas have the same transmission and the pupil disk appears to have a unit radius. The Airy pattern is again reproduced but, since the radius of the whole aperture is larger than in the case for $\theta = 0°$, the rings of the pattern have smaller diameter than in the case shown in Fig. 2(a). When $\theta = 135°$ both areas transmit with equal intensity, but there is a π phase-shift between them. The result is a zero intensity minima located at the center of the image plane.

Fig. 3 shows the behavior along the optical axis ($\rho = 0$). In this case the Jones vector for different values of W_{20} is obtained by multiplying the input Jones vector by the Jones matrix in Eq. (7), i.e.,

$$V_1(W_{20}) = \mathbf{F}(W_{20}) \cdot V_0 = \frac{\operatorname{sinc}(W_{20}/2)\exp(i\pi W_{20})}{2\sqrt{2}} \begin{pmatrix} 1 \\ \exp(i\pi W_{20}) \end{pmatrix}. \tag{13}$$

When there is no analyzer, the intensity along the axis is given, except for a constant factor, by $I(W_{20}) = \operatorname{sinc}^2(W_{20}/2)$ (lines named "NoA" in Fig. 3). The Jones vector $V_1(W_{20})$ shows that the state of polarization along the axis is in general elliptical with the ellipse axes oriented at $\pm 45°$. The local state of polarization along the axis is represented on top of Fig. 3(a) and (b). For $W_{20} = 0$, it is linear at 45°,

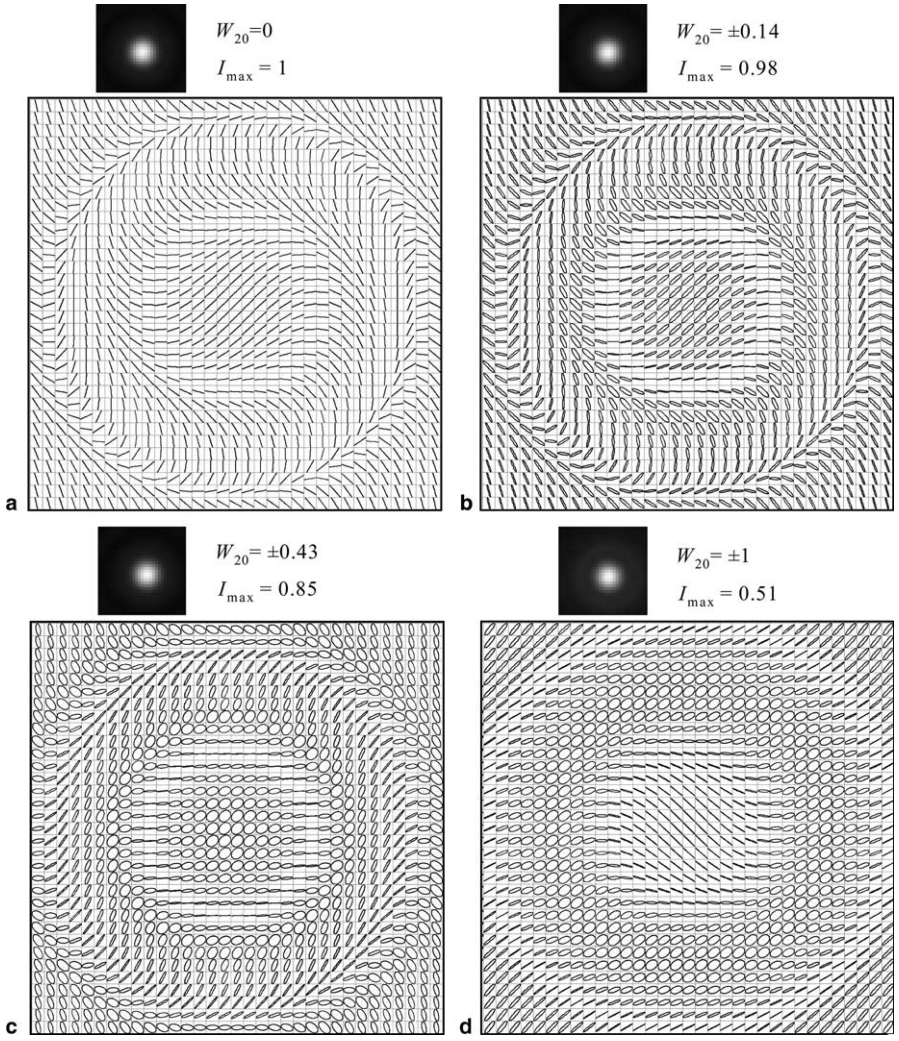

Fig. 4. Computer simulation for the intensity and polarization state distributions for defocused planes with $W_{20} = 0$, ± 0.14, ± 0.43 and ± 1. No analyzer is placed behind the pupil mask.

since the two polarization components are in phase. For $W_{20} = \pm 1$, there is a π phase-shift between the two components yielding linear polarization at 135°. For $W_{20} = \pm 0.5, \pm 1.5, \ldots$, the polarization becomes circular since the phase-shift between the two components is $\pi/2$ or $3\pi/2$.

When an analyzer with orientation θ is placed behind the aperture, the axial behavior depends on θ. As in the previous case, it is necessary to project the polarization states described by Eq. (13) onto the linear polarizer as $V_1^A(W_{20}) = \mathbf{R}(-\theta)\mathbf{P_0}\mathbf{R}(+\theta)V_1(W_{20})$. For $\theta = 0°$ and $\theta = 90°$ the intensity distribution along the axis is the same (see Fig. 3(a)). When $\theta = 45°$ the maximum in the image plane becomes more intense, while the depth of focus is narrower (Fig. 3(b)). Finally $\theta = 135°$, the intensity at the center is zero at the focal plane, and two maxima are obtained along the axis (Fig. 3(b)).

Finally, we performed simulations for different defocused planes. For that purpose we calculated the parameters F_{ij} in Eq. (1) for different values of W_{20}. Again the incident beam is considered linearly polarized at 45° and the input Jones vector is given by Eq. (8). Fig. 4 shows the results when no analyzer is present, corresponding to four different values of the defocused parameter W_{20}. For each case both the intensity and the polarization state distributions are shown. The distribution of polarization states is shown bigger in order to obtain a better visualization of the ellipses, but it corresponds to the same area shown at the intensity distributions. The intensity distributions are normalized in each case to the maximum value for a better visualization, but this value is indicated in the figure as $I_{\max}$. Fig. 4(a) corresponds to the best image plane ($W_{20} = 0$) and the results coincide with those in Fig. 2, i.e. the polarization is always linear but the orientations changes with the radial coordinate. However, as the system is defocused the polarization states become in general elliptical. The results on axis coincide with those shown in Fig. 3. Off axis, the polarization maps show rotational symmetry, but both azimuth and ellipticity change with the radial coordinate in a different way for different values of W_{20}. For example, for $W_{20} = \pm 0.43$ the states of polarization on the main central spot become circular (Fig. 4(c)), while they become linear oriented at $-45°$ for $W_{20} = \pm 1$ (Fig. 4(d)), i.e., orthogonal with respect to the best image plane (Fig. 4(a)). In this last case it is interesting to note that the polarization distributions for $W_{20} = \pm 1$ and for $W_{20} = 0$ are orthogonal only on axis, since in general light off-axis is elliptically polarized for $W_{20} = \pm 1$.

Fig. 5 shows the intensity distributions obtained when the analyzer is placed behind the pupil mask, oriented at angles $\theta = 0°$, 45°, 90° and 135°. Again, when $W_{20} = 0$ (left column), the results reproduce those presented in Fig. 2, and the results on axis coincide with those on Fig. 3. They are calculated as $I(\rho) = V_1^{A\dagger}(\rho, W_{20}) \cdot V_1^A(\rho, W_{20})$, where $V_1^A(\rho, W_{20})$ is the Jones vector at the observation plane. These intensity distributions correspond to the projection of the polarization distributions in Fig. 4 over the transmission angle θ, weighted with the intensity envelopes in Fig. 4. For instance, for $W_{20} = \pm 0.43$ the central spot intensity does not change when rotating the analyzer, since circular polarization states appear in this area (Fig. 4(c)). On the other hand, when $W_{20} = \pm 1$ the brightest central spot is obtained at $\theta = 135°$, while the center is dark for $\theta = 45°$, in accordance with the states of polarization shown in Fig. 4(d).

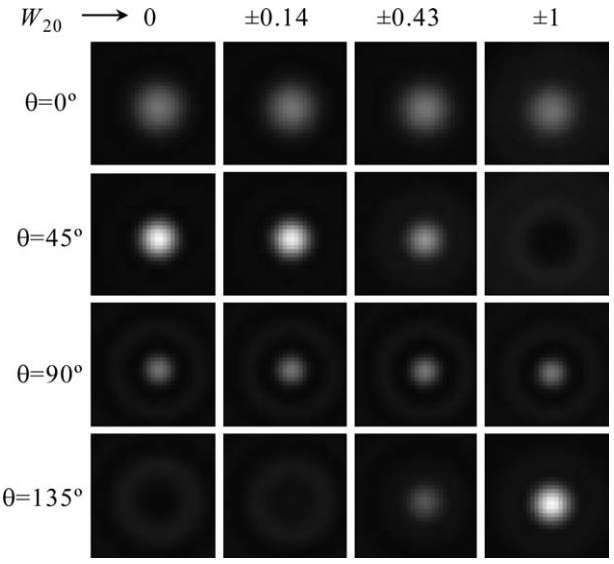

Fig. 5. Intensity distributions for defocused planes with $W_{20} = 0$, ± 0.14, ± 0.43 and ± 1, when an analyzer with orientation θ is placed behind the pupil mask. (a) $\theta = 0$, (b) $\theta = 45°$, (c) $\theta = 90°$ and (d) $\theta = 135°$.

4. Experimental realization with a twisted nematic liquid crystal display

We used a twisted nematic liquid crystal display to experimentally produce this kind of polarization pupil mask. In order to reproduce the polarization pupil described above, the LC-SLM was placed between two linear polarizers and we searched for a configuration leading to the highest contrast for two different addressed gray levels. In this situation the two emerging polarization states are linear, with orthogonal orientations. There is a phase difference between these two states, which was corrected placing a waveplate behind the SLM, oriented with its principal axes parallel to the polarization orientation of the two emerging linear states.

A clear circular aperture is selected to be the full aperture, and the LC-SLM is placed behind it producing the polarization distribution described in Fig. 1. The LC-SLM is located at the exit pupil of a zoom objective [5]. The numerical aperture is NA = 0.0036. Experimental results are shown in Fig. 6. The rows correspond to analyzer orientations $\theta = 0°$, 45°, 90° and 135°, and different columns correspond to different axial positions, measured in microns from the best image plane. These axial positions correspond to the values W_{20} used in the simulations of Figs. 4 and 5. In the central column ($z = 0$) the simulation

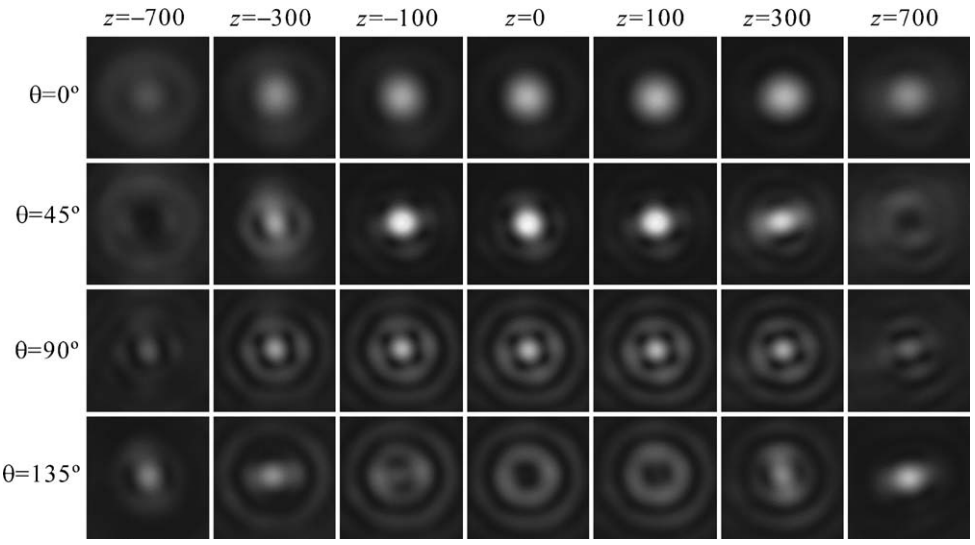

Fig. 6. Experimental results for analyzer placed at 0°, 45°, 90° and 135°, and for axial positions $z = 0$, ± 100, ± 300, and ± 700 μm.

results described in Fig. 2(a) and (b) are verified. The intensity at the center is maximum for $\theta = 45°$, it is reduced in the same way for $\theta = 0°$ and 90°, and it is zero for $\theta = 135°$. As expected, the radius of the central maximum is the smallest for $\theta = 90°$. These results show an excellent agreement with the numerical results in the first column in Fig. 5.

When the system is defocused, the experimental results also agree very well with the computer simulations shown in Figs. 3 and 4. In particular, it is interesting to note the agreement of the axial behavior. For $\theta = 0°$ the intensity on axis reduces following the curve in Fig. 3(a). For $\theta = 45°$ this reduction is much faster, and zero intensity at the center is found located at $z = \pm 700$ μm from the image plane, which is equivalent to $W_{20} = \pm 1$ (Fig. 3(b)). For $\theta = 90°$ and $\theta = 0°$ the intensity on axis is the same in both cases, in agreement with Fig. 3(a), although the behavior off-axis is very different in each case. Finally, for $\theta = 135°$ a zero is obtained in the center for $z = 0$, while two axial maxima appear. Again, all these experimental results show a very good agreement with the numerical predictions presented in Fig. 5 for defocused planes.

5. Conclusions

In summary, we have presented a Jones matrix based formalism to evaluate the response of an optical system with a nonuniform polarizing pupil mask. This formalism allows us to calculate the intensity and the local state of polarization. We have studied the properties of a polarization pupil mask with two regions: (1) the central disk transmits only a certain linear polarization; and (2) an annular aperture that surrounds it, with the same area, but transmitting the orthogonal linear polarization. We studied the three dimensional PSF of the optical imaging by employing the usual Jones matrix formalism and we obtained the intensity and the local state of polarization both in transverse planes and along the axis. The projection of these polarization images onto the orientation θ of an analyzer placed behind the pupil gives different behavior as a function of the angle θ. The pupil filter can be changed from being apodizing to be hyper-resolving simply by a rotation of the analyzer.

Finally, we have experimentally verified the numerical results by employing a twisted nematic LC-SLM. For that purpose, we searched for two different addressed gray levels that produce two orthogonal linear polarization states at the exit. We reproduced the above polarization pupil mask by addressing a binary signal with one of these gray levels addressed to the central disk, and the other one to the outer annulus. The presented experimental results show a very good agreement with the numerical simulations predicted by the theory. The use of such a programmable optical device will permit the generation of more complicated dynamical polarization distributions.

Acknowledgements

This work was supported by Ministerio de Ciencia y Tecnología from Spain (Refs: BFM2003-06273-C02-01/FISI and BFM2003-06273-C02-02/FISI). C. Iemmi acknowledges support from Universidad de Buenos Aires and CONICET (Argentina), and Generalitat de Catalunya (Project ACI 2003-42).

References

[1] C.S. Chung, H.H. Hopkins, J. Mod. Opt. 35 (1988) 1485.
[2] C.J.R. Sheppard, Z.S. Hegedus, J. Opt. Soc. Am. A 5 (1988) 643.
[3] J.A. Davis, J.C. Escalera, J. Campos, A. Márquez, M.J. Yzuel, C. Iemmi, Opt. Lett. 24 (1999) 628.
[4] A. Márquez, C. Iemmi, J.C. Escalera, J. Campos, S. Ledesma, J.A. Davis, M.J. Yzuel, Appl. Opt. 40 (2001) 2316.
[5] A. Márquez, C. Iemmi, J. Campos, J.C. Escalera, M.J. Yzuel, Opt. Exp. 13 (2005) 716.
[6] A. Márquez, C. Iemmi, I. Moreno, J.A. Davis, J. Campos, M.J. Yzuel, Opt. Eng. 40 (2001) 2558.

[7] J. Nicolás, J. Campos, M.J. Yzuel, J. Opt. Soc. Am. A 19 (2002) 1013.
[8] I. Moreno, A. Márquez, J.A. Davis, J. Campos, M.J. Yzuel, Opt. Pur. Apl. 38 (2) (2005) 1.
[9] Z. Zhuang, S.-W. Suh, J.S. Patel, Opt. Lett. 24 (1999) 694.
[10] J.A. Davis, D.E. McNamara, D.M. Cottrell, T. Sonehara, Appl. Opt. 39 (2000) 1549.
[11] A. Ghosh, K. Murata, A.K. Chakraborty, J. Opt. Soc. Am. A 5 (1988) 277.
[12] K. Bhattacharya, A.K. Chakraborty, A. Ghosh, J. Opt. Soc. Am. A 11 (1994) 586.
[13] Y. Unno, Appl. Opt. 37 (1988) 7241.
[14] F. Xiao, J. Yuan, G. Wang, Z. Xu, Appl. Opt. 43 (2004) 3415.
[15] I.J. Cooper, M. Roy, C.J.R. Sheppard, Opt. Exp. 13 (2005) 1066.
[16] I. Moreno, M.J. Yzuel, J. Campos, A. Vargas, J. Mod. Opt. 51 (2004) 2031.
[17] J.W. Goodman, Introduction to Fourier Optics, second ed., McGraw-Hill, New York, 1996.